Journal of Materials Chemistry A

PAPER

View Article Online
View Journal | View Issue

Cite this: J. Mater. Chem. A, 2015, 3, 16535

Facile simulation of carbon with wide pore size distribution for electric double-layer capacitance based on Helmholtz models†

Wei Hsieh,[a] Tzyy-Leng Allen Horng,[b] Hsin-Chieh Huang[a] and Hsisheng Teng*[ac]

This study reports on a facile method based on Helmholtz models for simulating the electric double-layer capacitance of various forms of carbon in aqueous H_2SO_4 and KOH and organic tetraethylammonium tetrafluoroborate/acetonitrile electrolytes. The proposed method combines cylindrical pore models for macropores and mesopores with the slit-pore model for micropores exhibiting constant surface-based capacitance (*C*/*S*). The pore structures and pore size distribution of carbon are analyzed by using a method based on non-local density functional theory (NLDFT). We then used data related to the capacitance of microporous carbon to evaluate the constant *C*/*S* values produced by distinct electrolytes in carbon micropores and to determine the molecule-sieving effect of the micropores. The constant *C*/*S* values obtained from the micropores suggest that the effective static dielectric constant at the electrode–electrolyte interface is proportional to the thickness of the ion-solvating layer. The *C*/*S* values in mesopores decreased with a decrease in the pore size due to the effects of wall-curvature confinement. For an aqueous electrolyte, the *C*/*S* values in micropores are larger than those in mesopores and macropores due to the compactness of the ion-solvating layers, which account for the higher dielectric constant in the micropores. Our simulation results regarding the capacitance values of each carbon are in excellent agreement with experimental data, thereby verifying the reliability of the proposed model. This model is capable of providing reliable, precise predictions of capacitance values and also reveals the mechanism underlying the double-layer formation of distinct pores and the interfacial properties associated with capacitive performance.

Received 8th June 2015
Accepted 7th July 2015

DOI: 10.1039/c5ta04125b

www.rsc.org/MaterialsA

1. Introduction

Electric double-layer capacitors (EDLCs) are promising electrochemical energy storage devices, in which the electrolyte–electrode interaction produces a long lifecycle, rapid charging,[1–5] and high power densities.[6,7] EDLCs store electrical charge *via* the electrostatic attraction between ions and the surface of electrodes. Porous carbon is currently the primary choice for EDLC electrodes, due to its low cost, acceptable conductivity, and high specific surface area. Matching the pore structure of electrodes with the properties of electrolyte ions is essential for improving the efficiency of charge storage. A number of models have been proposed to achieve this;[4,8–10] however, these are applicable only to electrodes that contain unimodal pores (*i.e.* a specific pore size). Researchers are yet to develop an integrated model applicable to the entire range of pore sizes with the ability to predict the capacitance of carbon electrodes containing multimodal pores.

In EDLCs, micropores (<2 nm) provide a large surface area for accommodating ions, while mesopores (2–50 nm) and macropores (>50 nm) facilitate relatively rapid ion transport.[11–17] Appropriate pore size distribution is crucial to optimizing the energy and power performance of EDLCs. This distribution depends on the electrolytes that are employed. Aqueous electrolytes such as KOH and H_2SO_4 have a limited potential window; however, they are safe and inexpensive.[1,3] Organic electrolytes, such as tetraethylammonium tetrafluoroborate ($TEABF_4$) in acetonitrile (AN), can be used over a wide range of voltages and are widely used in EDLCs, despite their volatility. In this study, we sought to develop the means to predict the capacitance of carbon materials incorporated with aqueous and organic electrolytes.

The Helmholtz theory outlines a double-layer structure applicable to the evaluation of capacitance. Macropores are far larger than electrolyte ions and solvent molecules. Double-layer capacitance based on the surface area of macropores can be

[a]Department of Chemical Engineering and Research Center for Energy Technology and Strategy, National Cheng Kung University, Tainan 70101, Taiwan. E-mail: hteng@mail.ncku.edu.tw; Fax: +886-6-23444; Tel: +886-6-2385371

[b]Department of Applied Mathematics, Feng Chia University, Taichung 40724, Taiwan

[c]Center for Micro/Nano Science and Technology, National Cheng Kung University, Tainan 70101, Taiwan

† Electronic supplementary information (ESI) available: The pore size distributions of carbons on the basis of incremental pore volume; the incremental capacitance values contributed by pores of varying sizes; the ion radii of electrolyte ions. See DOI: 10.1039/c5ta04125b

simulated using a flat-plate model, referred to as an EDLC model,[1–5,18] as follows:

$$C/S = \frac{\varepsilon_r \varepsilon_0}{d} \quad (1)$$

where C is the specific capacitance of the electrode, S is the specific surface area of the electrode, ε_r is the relative dielectric constant, ε_0 is the vacuum permittivity, and d is the thickness of the double-layer.

The dielectric constant can be dependent on frequency. However, here in EDLCs, the current is DC and we can neglect its frequency response; *i.e.*, the term 'dielectric constant' in this paper means effective static dielectric constant. Many polarization modes can contribute to the dielectric constant.[19] Nevertheless, in charged pores, no theory has been able to estimate the dielectric constant rigorously and correctly so far. As far as it can be fit well, the dielectric constant is a useful apparent parameter (a lump property for all kind of contributions).

As the pore size decreases, the curvature of the pores comes into play.[20] Previous studies proposed an electric double-cylinder capacitor (EDCC) model,[4,8,9] in which mesopores possess a cylindrical structure (with radius b), such that the ions form a circular double layer (with thickness d) on the pore wall (see Scheme 1). This EDCC model predicts the capacitance values according to the following equation:

$$C/S = \frac{\varepsilon_r \varepsilon_0}{b \ln\left(\frac{b}{b-d}\right)} \quad (2)$$

When confronted with cylindrical micropores, the ions do not form a circular structure, rather they line up along the axis of the cylindrical pore to form an electric wire-in-cylinder capacitor (EWCC).[4,8,9] This EWCC model postulates that a micropore accommodates an array of ions with an effective radius of a_0, the capacitance value of which can be obtained according to

$$C/S = \frac{\varepsilon_r \varepsilon_0}{b \ln\left(\frac{b}{a_0}\right)} \quad (3)$$

However, high-resolution electron microscopy provides evidence contradicting the EWCC model, showing that carbon micropores are actually slit-shaped, rather than cylindrical.[21] Apart from graphite, all carbons are quasi-crystalline because the covalent carbon atom network is not thermally stable and the carbon atoms in the network rearrange at high temperatures (>600 °C) to form a stable graphite-like lamellar constituent molecule.[22] Scanning transmission electron microscopy investigation demonstrated that the building blocks of microporous are randomly wrinkled graphene sheets.[23] High porosity carbons used as the electrodes for EDLCs are generally produced at temperatures above 700 °C and therefore these carbons consist of graphene sheets with their size and arrangement depending on the synthesis temperature. Treating carbon micropores as slits with varying widths is consistent with the realistic situation, even if the carbons have a strongly disordered structure.

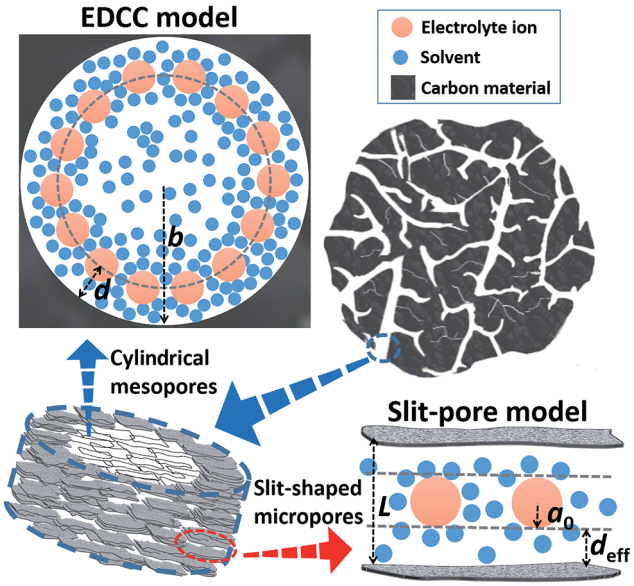

Scheme 1 The structural schematic of a porous carbon particle containing micropores and mesopores, in which the double layers are formed based on the EDCC model (eqn (2)) and slit-pore model (eqn (4)). The carbon particle comprises of stacked lamellar graphene sheets. Mesopores are charged to attract counter-ions surrounding the pore wall, behaving as an EDCC. As to slit-shaped micropores, a layer of counter-ions stay midway between two flat graphene sheets to form a sandwich capacitor when the pores are charged.

One previous study proposed a slit-pore model,[10] in which capacitance is derived using parallel plates to accommodate electrolyte ions (see Scheme 1); *i.e.*,

$$C/S = \frac{\varepsilon_r \varepsilon_0}{L/2 - a_0} = \frac{\varepsilon_r \varepsilon_0}{d_{eff}} \quad (4)$$

where L represents the width of slit pores and d_{eff} $(= L/2 - a_0)$ is the effective thickness of the double-layer. This slit-pore model is more realistic than the EWCC model for micropores in carbon materials. The EDLC, EDCC, EWCC and slit-pore models listed here are all Helmholtz models. The Gouy–Chapman–Stern model is more sophisticated for comprehensively describing EDL behavior;[24,25] however, the Gouy–Chapman–Stern model based on Boltzmann distribution is only suitable to describe cases of dilute concentration. Although many researchers have been working on the modification of the Stern–Gouy–Chapman model to include the steric effect,[26,27] we believe that Helmholtz models generally fit the experimental data quite well.

Most previous studies have evaluated surface-based capacitance C/S (generally in units of F m^{-2}) using the Brunauer–Emmett–Teller (BET) surface area. The C/S value presents an anomalous increase following a decrease in the pore size in the micropore regime.[28–30] Eqn (4) also predicts an increase in C/S with a decrease in pore size (L); however, it has been pointed out that the BET method produces incorrect assessments of the specific surface area in microporous materials.[31,32] In contrast, Density Functional Theory (DFT) provides a more realistic indication of the surface area and also provides wide-range pore size distributions based on adsorption isotherms. Non-local

DFT (NLDFT), which modifies fluid properties in confined spaces, is currently recommended by the International Standard Organization (ISO) for pore analysis.[33–37] One previous study compared the surface areas of carbide-derived carbons measured by the BET and NLDFT methods and ascribed the discrepancy between the two measures of surface areas to the breakdown of the BET method for small pores.[38] Centeno and Stoeckli *et al.* reported that when using the NLDFT to acquire the specific surface area, the C/S value is close to the constant for microporous carbon.[39–41] According to eqn (4), a constant C/S in micropores would indicate a decrease in the dielectric constant with a decrease in the pore size, which may be the result of the further desolvation of ions in smaller micropores.[42–45] Simulation studies reported that an increase in capacitance happens when the pore size equals the ion size,[42,46] but this can hardly be experimentally verified because of the very narrow pore-size range for the increase. As to pores with sizes smaller than the ion size, micropores exhibit molecule-sieving effects, which influence the accessibility of pores to electrolyte ions of specific sizes. This aspect of the issue has not been discussed previously in the evaluation of C/S values with regard to micropores.

Most of the carbon electrodes used in EDLCs contain pores of various sizes in order to optimize energy and power applications.[8,9] The NLDFT model has an advantage in the simultaneous analysis of pores over a wide range of sizes. Combining the above models for distinct pore size regimes results in a general model of electrodes with a multimodal pore size distribution, as follows:

$$C = \sum_{\text{micro}} (C/S) \times S_{\text{mi}} + \sum_{\text{meso}} \frac{\varepsilon_r \varepsilon_0}{b \ln\left(\frac{b}{b-d}\right)} \times S_{\text{me}} + \sum_{\text{macro}} \frac{\varepsilon_r \varepsilon_0}{d} \times S_{\text{ma}}. \quad (5)$$

Eqn (5) accommodates the information that the C/S values in micropores are constant, irrespective of pore size. This study validates eqn (5) by acquiring universal parameters to fit experimental data using specific carbon electrodes, including activated mesophase pitch (aMP) featuring an hierarchical pore structure,[47–49] microporous activated carbon fiber (aCF),[50,51] and templated mesoporous carbon (tMC).[13,14,52] We incorporated the surface area and pore size derived by the NLDFT method in the development of a universal model for predicting the capacitance of carbons containing multimodal pores in aqueous as well as organic electrolytes. The present study outlines the double-layer configurations found in porous carbons on the basis of Helmholtz theory. We also demonstrate that the size limitations placed on the slit-shaped micropores govern the prediction accuracy of the model in the organic electrolyte $TEABF_4$/AN.

2. Experimental

2.1. Materials

This study employed three types of porous carbon for the assembly of EDLCs: aMP, aCF, and tMC. aMP carbon was prepared by heating a mesophase pitch impregnated with KOH (KOH/pitch ratio of 4) at 800 °C for 1 h with subsequent neutralization.[47–49,53] The mesophase pitch used in this study was provided by China Steel Chemical Co., Taiwan. aCF carbon was obtained by milling a polyacrylonitrile-based activated carbon fiber cloth supplied by Challenge Carbon Technology Co., Taiwan.[51,53] tMC carbon was obtained by using a conventional silica-template method.[53] The carbon electrodes used in the assembled EDLCs consisted of 95 wt% porous carbon as the active material with 5 wt% multi-walled carbon nanotubes (UniRegion Bio-Tech, UR-NTM005; 10–30 nm in outer diameter and 5–15 μm in length) as a conductive medium.

Prior to characterization and electrochemical measurements, the carbon materials were heated to 900 °C and held under an argon atmosphere for 20 min to remove surface oxides, which have been shown to substantially reduce the electronic conductivity of carbon electrodes.

The electrolytes used in this study were aqueous solutions of 6 M KOH (Sigma-Aldrich, USA) and 1 M H_2SO_4 (Shimakyu, Japan) as well as an organic solution of 1.5 M $TEABF_4$ (Sigma-Aldrich, USA) in acetonitrile (J. T. Baker; USA).

2.2. Measurements

To determine the specific surface area and pore volume, nitrogen gas adsorption was performed using an adsorption apparatus (Micromeritics ASAP 2020 HD88, USA) at 77 K under N_2 at relative pressures (p/p_0) of 10^{-5} to 1. The samples were heated to 400 °C and held for 12 h prior to adsorption analysis. The apparent surface area (S_{BET}) of the samples was calculated using the Brunauer–Emmett–Teller (BET) equation. Realistic surface area (S_t), pore volume (V_t), and pore size distribution were analyzed using the NLDFT method,[54] under the assumption of a slit pore geometry.

We used a symmetrical two-electrode capacitor cell to examine the electrochemical performance of the porous carbon electrodes. To prepare the electrodes, a carbon specimen was dispersed in ethanol by sonication for 30 min before being applied to titanium foil (or nickel foil for use in the KOH electrolyte) with an active area of 1 cm^2 (2 mg, fixed under stress without using a binder). The symmetrical cells comprised two carbon electrodes, facing each other and sandwiching a cellulose filter paper as a separator. The cells were assembled under stress to ensure intimate contact at the carbon–carbon and carbon–collector foil interfaces. Binder-free electrodes with strong contact between the carbon particles and the current collector provide an accurate indication of the capacitance of active materials. All electrochemical measurements were performed at room temperature (approximately 25 °C). Cell performance was recorded using an electrochemical analyzer (Solartron Analytical, Model 1470E, UK) by performing galvanostatic charge–discharge measurements between 0–1 and 0–2 V for the aqueous and organic electrolytes, respectively. Capacitance values in all of the electrolytes were obtained from stabilized discharge at a current density of 0.125 A g^{-1}, which is close to the current values used in previous studies.[24,55–57]

3. Results and discussion

Fig. 1 presents the N_2 adsorption–desorption isotherms of aCF, tMC, and aMP. The isotherms of aCF (Fig. 1a) display strong adsorption and early saturation at low pressures, which is indicative of a microporous morphology.[58] The isotherms of aMP (Fig. 1b) show abrupt adsorption at low pressures followed by gradual adsorption with an increase in pressure, indicative of wide pore size distribution. The appearance of hysteresis at relative pressures above 0.45 confirms the contribution of mesoporosity. The tMC sample (Fig. 1c) is typical of mesoporous carbon, in which no isotherm plateaus are present and a hysteresis loop resulting from capillary condensation can be clearly observed.

Fig. 2 presents the pore size distribution determined by applying NLDFT calculation to the isotherm-related data in Fig. 1. Pore size distribution is illustrated in terms of incremental surface area to facilitate the calculation of C/S values. For comparison, Fig. S1 in the ESI† presents pore size distribution on the basis of incremental pore volume. Table 1 lists the total surface area and pore volume determined by using the NLDFT method (*i.e.*, S_t and V_t) as well as the micropore surface area (S_{mi}) and micropore volume contribution (X_{mi}) to V_t. The BET surface area (S_{BET}) is also listed; however, the values determined using the NLDFT method tend to be more realistic for carbon containing micropores.[31,32,54] The S_t values measured for aCF, aMP, and tMC are 763, 1750, and 930 g^{-2}, respectively. The S_{BET} values exceed S_t. The X_{mi} values are indicative of the microporous and mesoporous features of aCF and tMC, respectively, as well as heterogeneity in the porosity of aMP.

We sought to simulate the capacitive behavior resulting from micropores using a slit-pore model,[10] despite the fact that a number of previous studies have employed the EWCC model.[4,8,9] Most carbon micropores are believed to be locally slit-shaped pores, which is inherent to the nature of graphite. Mesopores are cylinder-shaped features created by perforating the structure of activated carbon. Mesopores are commonly modeled using the EDCC model. Scheme 1 illustrates the

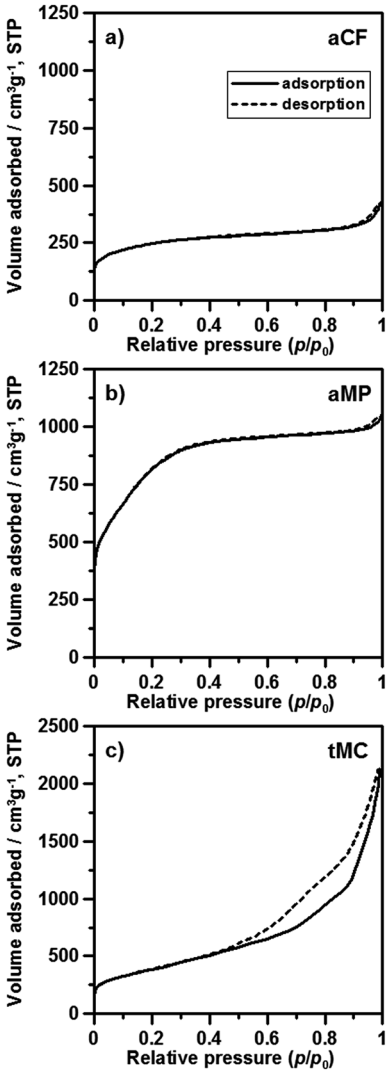

Fig. 1 The N_2 adsorption–desorption isotherms of different carbons: (a) aCF; (b) aMP; (c) tMC.

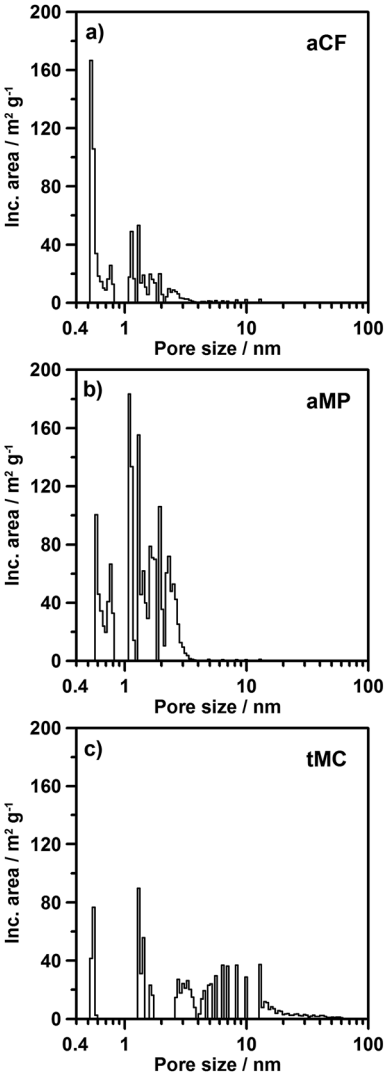

Fig. 2 The NLDFT-calculated pore size distributions of the carbons presented in terms of incremental surface area: (a) aCF; (b) aMP; (c) tMC.

Table 1 Pore structure of the aCF, aMP, and tMC carbons. S_t and V_t represent the surface area and pore volume determined by the NLDFT method, and S_{mi} and X_{mi} represent the micropore surface area and micropore volume contribution to V_t. S_{BET} represents the surface area determined by the BET method

Carbon	S_t ($m^2\ g^{-1}$)	S_{mi} ($m^2\ g^{-1}$)	V_t ($cm^3\ g^{-1}$)	X_{mi} (%)	S_{BET} ($m^2\ g^{-1}$)
aCF	763	680	0.60	51	877
aMP	1750	1390	1.50	63	2700
tMC	930	340	3.10	7	1250

Table 2 The relative dielectric constant (ε_r) and double-layer thickness (d) values of the EDLC and EDCC models employed for macropores and mesopores, respectively, in different electrolytes and the constant C/S values for micropores

Electrolyte	ε_r [a]	d [a] (nm)	C/S ($F\ m^{-2}$)
$TEABF_4$/AN	11.6	0.820	0.125
H_2SO_4	17.4	0.900	0.194
KOH	12.5	0.775	0.174

[a] The values were obtained from ref. 18 and 19.

schematic structure of a porous carbon particle containing micro- and mesopores. Macropores are not presented in this schematic because they contribute little to the overall capacitance, due to their low surface area (see Fig. 2). Mesopores are actually cylindrical channels with walls assembled by the stacking of lamellar graphene sheets. The slits in the stacked graphene sheets form micropores. The charge of mesopores attracts counter-ions, which then surround the pore walls (Scheme 1), and behave as an EDCC. The ions are solvated by solvent molecules at a fixed distance d (*i.e.*, the double-layer thickness) from the pore wall. As for the slit-shaped micropores, a layer of counter-ions remains sandwiched midway between the two flat graphene sheets, resulting in the formation of a capacitor when the pores are charged. Generally, the ions in micropores are only partially solvated due to the confinement effect, wherein the thickness of the solvation shell decreases with the reducing width of the slit. The distance between ions and the pore wall (d_{eff}) and the associated dielectric constant therefore depend on the pore size and vary at the same degree. The size threshold dividing cylindrical mesopores from slit-shaped micropores is critical to the simulation of capacitance. This study adopted the conventional 2 nm threshold, which is roughly the size of a fully solvated ion.

We calculated the C/S values using the surface area obtained using the NLDFT model, which are applicable to the entire range of pore sizes associated with porous carbon.[54] In the simulation of capacitance values for macropores and mesopores, we used the EDLC and EDCC models (eqn (1) and (2), respectively) in conjunction with the ε_r and d values obtained from a regression of literature-reported data.[8,9] Table 2 presents the ε_r and d values of the EDLC and EDCC models for the electrolytes in the present study.[8,9] Fig. 3 presents the variations in predicted C/S with the pore size, which were obtained by applying the ε_r and d values to the EDCC model (eqn (2)) for mesopores (2–50 nm). The dashed lines in Fig. 3 represent the constant C/S values calculated for macropores (>50 nm) using the EDLC model (eqn (1)) using the ε_r and d values listed in Table 2. For large mesopores (~50 nm), the EDCC model produces capacitance values asymptotically close to the values obtained for macropores using the EDLC. The capacitance of mesopores presents a decreasing trend with a decrease in the pore size due to the increasing influence of wall curvature on the ion layer over the pore walls. When the size of the pores decreased from the mesopore regime to that of the micropore (<2 nm), a dramatic change in the C/S value was observed at the regime border (*i.e.*, at 2 nm) due to a transformation in the configuration of pores from cylindrical to slit-shaped, as illustrated in Scheme 1.

In the simulation of capacitance for micropores, we adopted the constant-C/S model using C/S values acquired from experimental data obtained in the present study due to divergences in the constant C/S values reported by previous studies.[42–45] In contrast, a number of previous studies have used S_{BET} for the simulation of C/S values in micropores, which resulted in a sharp increase in capacitance with a decrease in the pore size.[31,32] In a systematic study on a large variety of carbon materials, Centeno *et al.* showed that the use of the BET model resulted in an increased underestimation of the surface area (relative to that determined by NLDFT) with a decrease in the pore size.[40,41] This helps to explain the increase in C/S following a decrease in the size of micropores, which was observed in previous studies using S_{BET} for calculation.[31,32]

Fig. 4 presents the voltage–time curves of the cells charged and discharged at 0.125 A g^{-1} (or 0.5 mA cm^{-2}) in aqueous and organic electrolytes. The voltage ranges were as follows: the organic $TEABF_4$/AN was 2 V (Fig. 4a) and the aqueous H_2SO_4 and KOH were 1 V (Fig. 4b and c). All of the cells exhibited standard capacitive behavior within the applied voltage ranges. We calculated the specific electrode capacitance (C) according to $C = 4 \times I \times t_d/(M \times \Delta V)$, where I is the discharge current, t_d is the discharge time, M represents the total carbon mass of two symmetric electrodes, and ΔV is the voltage difference in discharge excluding the IR drop. Fig. 4 also presents the C values of the carbon electrodes obtained in the various electrolytes. The capacitance values produced in the organic electrolyte were smaller than those in the aqueous electrolyte, which could be attributed to the difference in size between the electrolyte ions and in dielectric constant between the solvent molecules.[59–61]

This study sought to take advantage of the microporosity of aCF by using the capacitance data of aCF to evaluate the constant C/S values produced by the electrolytes in the carbon micropores. We employed eqn (5) by incorporating the specific capacitance (Fig. 4) and NLDFT surface area data of aCF (Fig. 2) with the capacitance values for the meso- and macropores in

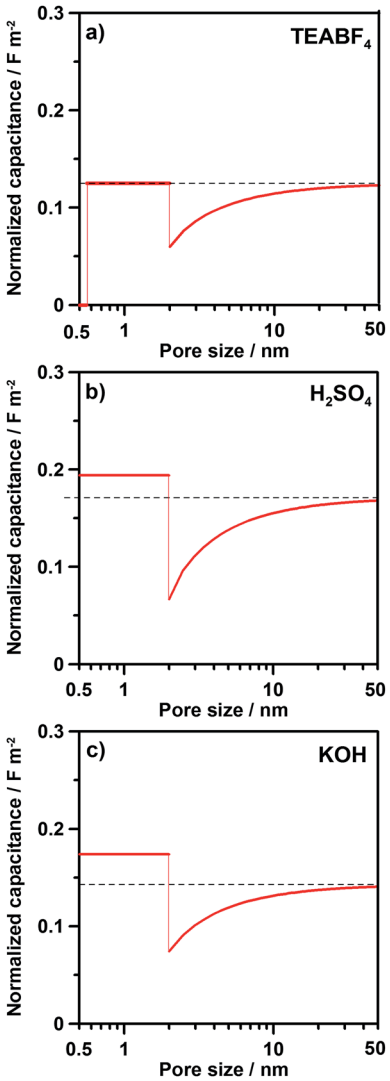

Fig. 3 Variation of predicted *C*/*S* values with the pore size by applying the EDLC model (eqn (1)) for macropores (>50 nm) and the EDCC model (eqn (2)) for mesopores (2–50 nm), and by using the capacitance data of aCF to evaluate the constant *C*/*S* values for micropores (<2 nm). The ε_r and *d* values listed in Table 2 are used for the EDLC and EDCC models. The solid lines represent the *C*/*S* variation with the pore size in the micropore and mesopore regimes and the dashed lines represent the constant *C*/*S* values for macropores.

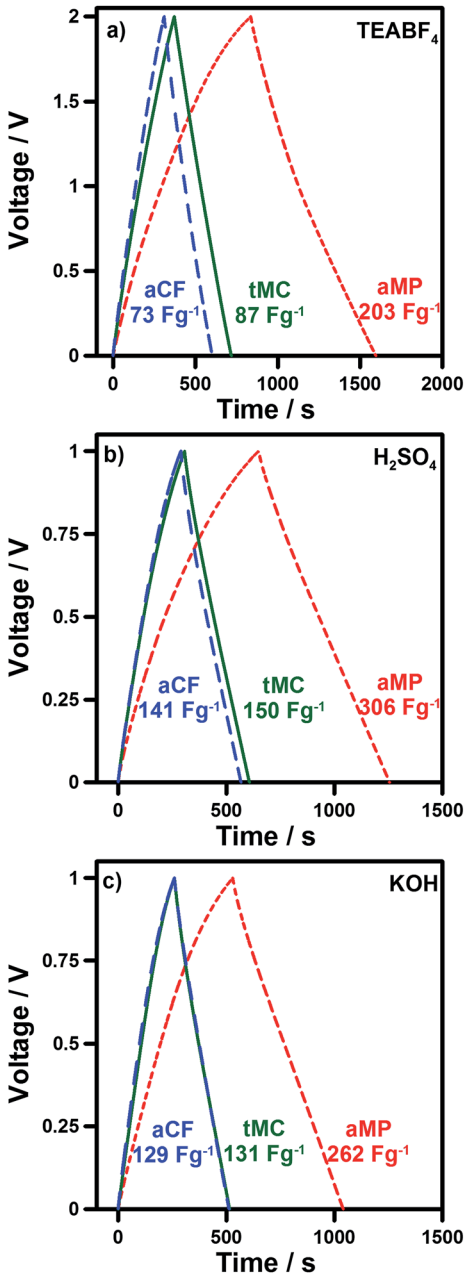

Fig. 4 The voltage–time curves of the cells charged and discharged at 0.125 A g^{-1} in the organic and aqueous electrolytes: (a) organic $TEABF_4$/AN with a 2 V voltage range; (b) aqueous H_2SO_4 with a 1 V voltage range; (c) aqueous KOH with a 1 V voltage range. The specific capacitance values, *C*, determined from discharge are presented in this figure.

aCF (Fig. 3) to obtain the constant *C*/*S* values for micropores (listed in Table 2). These *C*/*S* values are as follows: aqueous H_2SO_4 (0.194 F m^{-2}), KOH (0.174 F m^{-2}), and organic $TEABF_4$/AN (0.125 F m^{-2}). We excluded pores smaller than the average size of TEA^+ and BF_4^- (*i.e.*, 0.56 nm) in *C*/*S* calculations when the cells were assembled using organic $TEABF_4$/AN. Thus, the *C*/*S* values obtained in this study were larger than those reported previously.[39–41] The constant *C*/*S* values for micropores are plotted as solid lines within 0.5–2 nm in Fig. 3. The variations in capacitance in Fig. 3 reveal that cylindrical mesopores exhibit pore-size dependent *C*/*S* due to the influence of wall curvature. In contrast, the walls of micropores and macropores, which are relatively flat when compared to the size of the ions, exhibit constant *C*/*S* values irrespective of pore size.

The applicability of the proposed multimodal model (*i.e.*, eqn (5) in conjunction with NLDFT pore analysis and the parameters listed in Table 2) was evaluated by predicting the capacitance values of aMP and tMC, which have pore structures very different from that of aCF. Based on the pore size distribution in Fig. 2, Fig. S2 of the ESI† presents the incremental capacitance values contributed by the various pores sizes in the various electrolytes in this study. Fig. 5 shows the plot of the data in Fig. S2† as cumulative capacitance. Micropores (<2 nm)

contributed 95% of the total capacitance in aCF and most of the capacitance in aMP. In contrast, most of the contribution to capacitance in tMC was from mesopores. Fig. 5 also presents the total specific capacitance values measured in the charge–discharge experiments (Fig. 4). The simulation data are in good agreement with the experimental data, although some minor differences are present likely due to the divergence in the meso-/micropore regime border for different carbon forms. Nevertheless, the consistence between simulation and experiments confirms the reliability of the parameters (Table 2) as well as the feasibility of the proposed Helmholtz model (eqn (5)).

For pores smaller than 1 nm, the simulation in Fig. 5 presents larger cumulative capacitance values for aCF than for aMP in aqueous electrolytes. This can be explained by the large surface area of aCF in this pore size regime (Fig. 2). However, aMP exhibited higher capacitance in the $TEABF_4$/AN electrolyte than did aCF, due to the fact that in the present model, some small micropores ($L < 0.56$ nm) in aCF are inaccessible to ions in the electrolyte, based on the mean radius of ions listed in Table S1 of the ESI†. The accuracy attained in the prediction of capacitance using various forms of carbon justifies the existence of the molecule-sieving effect for using this organic electrolyte in capacitors. Fig. 5 also reveals that the high C/S values obtained for micropores in aqueous electrolytes (Fig. 3) produced similar capacitance values for aCF and tMC, despite the fact that the microporous aCF has a smaller S_t. In $TEABF_4$/AN, aCF presents smaller capacitance values than tMC, because the C/S value for micropores is nearly the same as the asymptotic value of mesopores (Fig. 3). The model proposed in this study explicitly elucidates the influence of the electrolyte type on capacitive performance in various forms of carbon.

The constant capacitance value observed with micropores suggests that the dielectric constant of the electrode–ion interface decreases with the pore size, in accordance with the slit-pore model (eqn (4)). Several previous studies also observed a decrease in the dielectric constant of aqueous and organic solutions within a confined space due to ion desolvation.[43–45] Some simulation studies on EDLCs have demonstrated that the pore-width dependent dielectric constant, due to varying thickness of the solvation shell, may modulate the capacitance to cause a constant C/S in micropores.[42,46] In contrast, simulations for pure ionic liquids show a capacitance increase with decreasing pore size.[62,63] The constant C/S leads to the conclusion that the ε_r/d_{eff} value is essentially constant in micropores; *i.e.*, the dielectric constant is proportional to the thickness of the solvation shell for ions. This linear correlation indicates that the concentration of solvent molecules in such a confined space decreases with a decrease in the width of the slit; thereby weakening the polarizability of the interface. Using eqn (4), the ε_r/d_{eff} values of micropores are as follows: $TEABF_4$/AN (0.125 F m^{-2}) and aqueous H_2SO_4 (0.194 F m^{-2}) and KOH (0.174 F m^{-2}). Fig. 6a presents the variations in ε_r with d_{eff}. We postulate that the interfacial ions are entirely desolvated when ε_r reaches unity. The d_{eff} value at $\varepsilon_r = 1$ may represent the interfacial distance between naked ions and pore walls. Fig. 6a ranks the interfacial distances in the various electrolytes as follows: aqueous-H_2SO_4 < aqueous-KOH < $TEABF_4$/AN. Previous studies showed that the affinities between the ions and solvent molecules are ranked as aqueous-H_2SO_4 > aqueous-KOH > $TEABF_4$/AN.[61,64,65] The stronger the affinity, the smaller the interfacial distance is for the stabilization of the naked ions in micropores. The strong ion-solvent affinity of the aqueous H_2SO_4 solution indicates a high concentration of solvent molecules within the interfacial d_{eff} zone, which accounts for the large dielectric constant and therefore the high C/S values for carbons immersed in aqueous H_2SO_4.

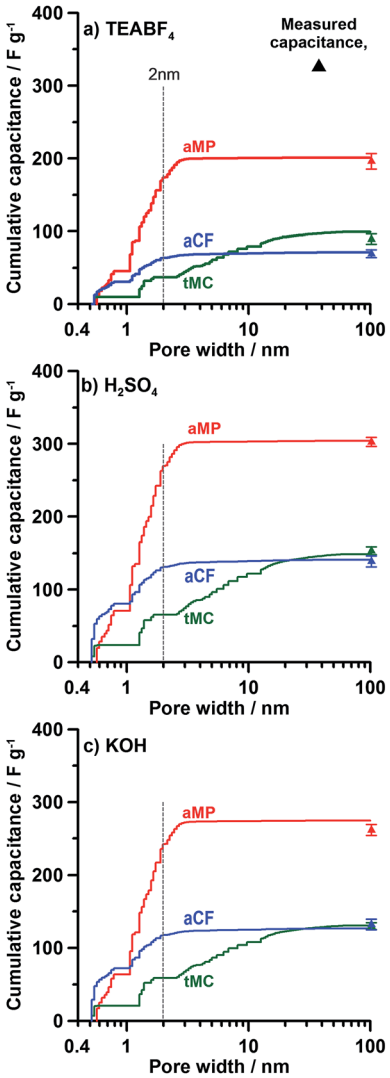

Fig. 5 Variation of the cumulative capacitance with pore size simulated by incorporating the pore size distribution (Fig. 2) and C/S (Fig. 3) data into eqn (5) for different electrolytes: (a) organic $TEABF_4$/AN; (b) aqueous H_2SO_4; (c) aqueous KOH. The total capacitance values measured from the charge–discharge experiments (Fig. 4) are presented in this figure, as the triangle symbols, for comparison.

Incorporating the results from Fig. 6a into the relationship of $d_{eff} = L/2 - a_0$ under the assumption that a_0 corresponds to the mean radius of ions in the electrolytes (see Table S1†) makes it possible to estimate the interfacial ε_r values for micropores of various sizes in a variety of electrolytes. Fig. 6b ranks the interfacial ε_r values for micropores of the same size as follows:

aqueous-H_2SO_4 > aqueous-KOH > $TEABF_4$/AN. This ranking is in accordance with the order of the micropore C/S values in these electrolytes. The ranking of the ε_r values in micropores is identical to that in the mesopores and macropores (Table 2). It should be noted that ε_r in micropores at L close to 2 nm (see Fig. 6b) is close to the value for mesopores and macropores, as shown in Table 2. This consistency and continuity in ε_r values derived from very different models for the various pore-size regimes validates the use of these models for predictions of capacitance. Nevertheless, for aqueous electrolytes, ε_r in micropores at L close to 2 nm is somewhat larger than its counterpart for mesopores and macropores. In cases with strong ion-solvent affinity, the confined space within micropores may result in the compaction of solvating solvent molecules, resulting in increased ε_r values. The compact solvation layer in micropores led to an increase in C/S values, relative to those obtained for mesopores and macropores (Fig. 3). This confinement associated with the aqueous electrolyte could increase the C/S value in micropores relative to the asymptotic C/S value in mesopores, as shown in Fig. 3.

Our method based on Helmholtz theory provides a facile means for elucidating the double-layer formation mechanism in carbons with wide pore size distribution. The model parameters explicitly elucidate the interface properties associated with the solvation layers for ions. We expect that this model could be applied to other carbon/electrolyte systems for the optimization of EDLCs with regard to energy performance.

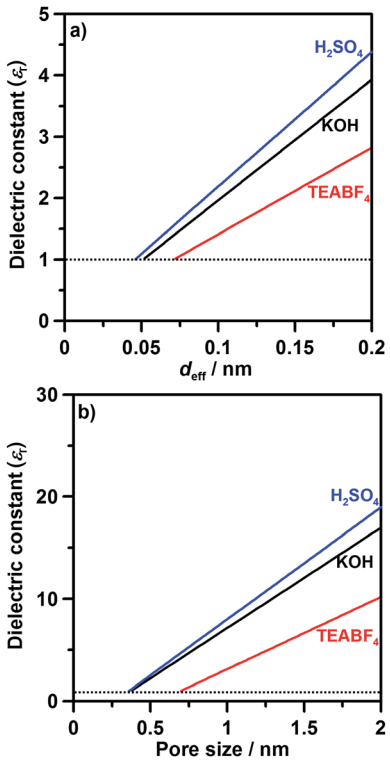

Fig. 6 Variation of the relative dielectric constant ε_r in micropores with: (a) effective double-layer thickness, d_{eff}; (b) pore width, L. The interfacial ions can be postulated to be completely desolvated when ε_r reaches a value of unity, which is notified by the dashed lines.

4. Summary and conclusions

This study established a model for the simulation of double-layer capacitance in carbon materials with wide pore size distribution in organic and aqueous electrolytes. Our model is based on Helmholtz theory, employing surface area and pore size determined using the NLDFT method for the estimation of C/S values. The simulated capacitance values of three distinct forms of carbon are in excellent agreement with the experimental data, thereby verifying the reliability and feasibility of the proposed model. This capacitance model is applicable to cylindrical mesopores and slit-shaped micropores; however, macropores contribute little to the specific surface area and therefore have little effect on capacitance. The C/S value of mesopores decreases with a decrease in the pore size due to an increase in the influence of wall curvature on ion layering. Micropores exhibit constant C/S values irrespective of pore size, which indicates that, in the confined space of micropores, the degree of ion solvation decreases with a decrease in the pore size to lower the dielectric constant at the wall–electrolyte interface. The aqueous electrolytes, H_2SO_4 and KOH, produce higher C/S values than the organic electrolyte, $TEABF_4$/AN, due to their stronger affinity to solvent molecules, which results in a larger interfacial dielectric constant. This model reveals the molecule-sieving effect of micropores, in which pores with sizes smaller than 0.56 nm did not contribute to capacitance in the organic electrolyte. This facile simulation interprets the double-layer formation mechanism and reveals properties of the electrode–electrolyte interface that govern the charge storage performance.

Acknowledgements

This research was supported by the Ministry of Science and Technology, Taiwan (101-2221-E-006-243-MY3, 101-2221-E-006-225-MY3, 103-3113-E-006-009, and 102-3113-E-006-002), and by the Ministry of Education, Taiwan, The Aim for the Top University Project to the National Cheng Kung University.

Reference

1 R. Kötz and M. Carlen, *Electrochim. Acta*, 2000, **45**, 2483–2498.
2 A. Burke, *J. Power Sources*, 2000, **91**, 37–50.
3 P. Simon and Y. Gogotsi, *Acc. Chem. Res.*, 2013, **46**, 1094–1103.
4 P. Simon and Y. Gogotsi, *Nat. Mater.*, 2008, **7**, 845–854.
5 B. E. Conway, in *Electrochemical Supercapacitors: Scientific Fundamentals and Technological Applications*, Kluwer Academic Plenum, New York, 1999.
6 D. Pech, M. Brunet, H. Durou, P. Huang, V. Mochalin, Y. Gogotsi, P. Taberna and P. Simon, *Nat. Nanotechnol.*, 2010, **5**, 651–654.
7 M. F. El-Kady, V. Strong, S. Dubin and R. B. Kaner, *Science*, 2012, **335**, 1326–1330.
8 J. Huang, B. G. Sumpter and V. Meunier, *Angew. Chem., Int. Ed.*, 2008, **47**, 520–524.

9 J. Huang, B. G. Sumpter and V. Meunier, *Chem.–Eur. J.*, 2008, **14**, 6614–6626.
10 G. Feng, R. Qiao, J. Huang, B. G. Sumpter and V. Meunier, *ACS Nano*, 2010, **4**, 2382–2390.
11 P. Simon and A. Burke, *J. Electrochem. Soc.*, 2008, **17**, 38–43.
12 M. Karthik, E. Redondo, E. Goikolea, V. Roddatis, S. Doppiu and R. Mysyk, *J. Phys. Chem. C*, 2014, **118**, 27715–27720.
13 W. Xing, S. Z. Qiao, R. G. Ding, F. Li, G. Q. Lu, Z. F. Yan and H. M. Cheng, *Carbon*, 2006, **44**, 216–224.
14 K. Xia, Q. Gao, J. Jiang and J. Hu, *Carbon*, 2008, **46**, 1718–1726.
15 D. Saha, E. A. Payzant, A. S. Kumbhar and A. K. Naskar, *ACS Appl. Mater. Interfaces*, 2013, **5**, 5868–5874.
16 L. Zhang, X. Yang, F. Zhang, G. Long, T. Zhang, K. Leng, Y. Zhang, Y. Huang, Y. Ma, M. Zhang and Y. Chen, *J. Am. Chem. Soc.*, 2013, **135**, 5921–5929.
17 S. Yoon, J. Lee, T. Hyeon and S. M. Oh, *J. Electrochem. Soc.*, 2000, **147**, 2507–2512.
18 E. Frackowiak, *Phys. Chem. Chem. Phys.*, 2007, **9**, 1774–1785.
19 M. V. Fedorov and A. A. Kornyshev, *Chem. Rev.*, 2014, **114**, 2978–3036.
20 J. Huang, B. G. Sumpter and V. Meunier, *J. Mater. Res.*, 2010, **25**, 1525–1531.
21 J. R. Fryer, *Carbon*, 1981, **19**, 431–439.
22 H. Marsh and M.-A. D. Díaz-Estébanez, in *Sciences of Carbon Materials*, Universidad de Alicante, Spain, 2000, p. 374.
23 J. Guo, J. R. Morris, Y. Ihm, C. I. Contescu, N. C. Gallego, G. Duscher, S. J. Pennycook and M. F. Chisholm, *Small*, 2012, **8**, 3283–3288.
24 O. Stern, *Z. Electrochem.*, 1924, **30**, 508–516.
25 K. B. Oldham, *J. Electroanal. Chem.*, 2008, **613**, 131–138.
26 I. Borukhov, D. Andelman and H. Orland, *Phys. Rev. Lett.*, 1997, **79**, 435–438.
27 M. S. Kilic, M. Z. Bazant and A. Ajdari, *Phys. Rev. E: Stat., Nonlinear, Soft Matter Phys.*, 2007, **75**, 021502.
28 J. Chmiola, G. Yushin, Y. Gogotsi, C. Portet, P. Simon and P. L. Taberna, *Science*, 2006, **313**, 1760–1763.
29 B. Daffos, P. L. Taberna, Y. Gogotsi and P. Simon, *Fuel Cells*, 2010, **10**, 819–824.
30 C. Largeot, C. Portet, J. Chmiola, P.-L. Taberna, Y. Gogotsi and P. Simon, *J. Am. Chem. Soc.*, 2008, **130**, 2730–2731.
31 J. Rouquérol, D. Avnir, C. W. Fairbridge, D. H. Everett, J. M. Haynes, N. Pernicone, J. D. F. Ramsay, K. S. W. Sing and K. K. Unger, *Pure Appl. Chem.*, 1994, **66**, 1739–1758.
32 K. S. W. Sing and R. T. Williams, *Part. Part. Syst. Charact.*, 2004, **21**, 71–79.
33 ISO-15901-3, Pore size distribution and porosity of solid materials by mercury porosimetry and gas adsorption, Analysis of micropores by gas adsorption, 2007.
34 J. Landers, G. Y. Gor and A. V. Neimark, *Colloids Surf., A*, 2013, **437**, 3–32.
35 P. Tarazona, *Mol. Phys.*, 1987, **60**, 573–595.
36 N. A. Seaton, J. P. R. B. Walton and N. Quirke, *Carbon*, 1989, **27**, 853–861.
37 C. Lastoskie, K. E. Gubbins and N. Quirke, *Langmuir*, 1993, **9**, 2693–2702.
38 J. C. Palmera, A. Llobetb, S. H. Yeonc, J. E. Fischerd, Y. Shie, Y. Gogotsic and K. E. Gubbins, *Carbon*, 2010, **48**, 1116–1123.
39 T. A. Centeno and F. Stoeckli, *Electrochim. Acta*, 2011, **56**, 7334–7339.
40 F. Stoeckli and T. A. Centeno, *J. Mater. Chem. A*, 2013, **1**, 6865–6873.
41 T. A. Centeno, O. Sereda and F. Stoeckli, *Phys. Chem. Chem. Phys.*, 2011, **13**, 12403–12406.
42 S. Kondrat, A. Kornyshev, F. Stoeckli and T. A. Centeno, *Electrochem. Commun.*, 2013, **34**, 348–350.
43 A. Senapati and A. Chandral, *J. Phys. Chem. B*, 2001, **105**, 5106–5109.
44 B. E. Conway, J. O. 'M. Bockris and I. A. Ammar, *Trans. Faraday Soc.*, 1951, **47**, 756–766.
45 L. S. Palmer, A. Cunliffe and J. M. Hough, *Nature*, 1952, **170**, 796.
46 D. Jiang, Z. Jin, D. Henderson and J. Wu, *J. Phys. Chem. Lett.*, 2012, **3**, 1727.
47 T. C. Weng and H. Teng, *J. Electrochem. Soc.*, 2001, **148**, A368–A373.
48 M. F. Hsueh, C. W. Huang, C. A. Wu, P. L. Kuo and H. Teng, *J. Phys. Chem. C*, 2013, **117**, 16751–16758.
49 C. W. Huang, C. T. Hsieh, P. L. Kuo and H. Teng, *J. Mater. Chem.*, 2012, **22**, 7314–7322.
50 H. Y. Liu, K. P. Wang and H. Teng, *Carbon*, 2005, **43**, 559–566.
51 C. W. Huang, C. A. Wu, S. S. Hou, P. L. Kuo, C. T. Hsieh and H. Teng, *Adv. Funct. Mater.*, 2012, **22**, 4677–4685.
52 S. A. Al-Muhtaseb and J. A. Ritter, *Adv. Mater.*, 2003, **15**, 101–114.
53 H. C. Huang, C. W. Huang, C. T. Hsieh and H. Teng, *J. Mater. Chem. A*, 2014, **2**, 14963–14972.
54 T. A. Centeno and F. Stoeckli, *Carbon*, 2010, **48**, 2478–2486.
55 C. Vix-Guterl, E. Frackowiak, K. Jurewicz, M. Friebe, J. Parmentier and F. BUguin, *Carbon*, 2005, **43**, 1293–1302.
56 G. Lota, T. A. Centeno, E. Frackowiak and F. Stoechkli, *Electrochim. Acta*, 2008, **53**, 2210–2216.
57 G. Gryglewicz, J. Machnikowski, E. Lorenc-Grabowska, G. Lota and E. Frackowiak, *Electrochim. Acta*, 2005, **50**, 1197–1206.
58 F. Rouquerol, J. Rouquerol and K. Sing, in *Adsorption by Powders and Porous Solids*, Academic Press, London, 1999.
59 Y. Marcus, *Biophys. Chem.*, 1994, **51**, 111–127.
60 D. Jiang, Z. Jin, D. Henderson and J. Wu, *J. Phys. Chem. Lett.*, 2012, **3**, 1727–1731.
61 G. Feng, J. Huang, B. G. Sumpter, V. Meunier and R. Qiao, *Phys. Chem. Chem. Phys.*, 2010, **12**, 5468–5479.
62 D. Jiang, Z. Jin and J. Wu, *Nano Lett.*, 2011, **11**, 5373–5377.
63 S. Kondrat, C. R. Pérez, V. Presser, Y. Gogotsi and A. A. Kornyshev, *Energy Environ. Sci.*, 2012, **5**, 6474–6479.
64 K. W. Frese, Jr., *J. Phys. Chem.*, 1989, **93**, 5911–5916.
65 A. V. Marenich, R. M. Olson, C. P. Kelly, C. J. Cramer and D. G. Truhlar, *J. Chem. Theory Comput.*, 2007, **3**, 2011–2033.

Electronic Supplementary Information

Facile Simulation of Electric Double Layer Capacitance for Carbons with Wide Pore Size Distributions Based on Helmholtz Models

Wei Hsieh,[1] Tzyy-Leng Allen Horng,[2] Hsin-Chieh Huang,[1] and Hsisheng Teng[1,3,*]

[1]Department of Chemical Engineering and Research Center for Energy Technology and Strategy, National Cheng Kung University, Tainan 70101, Taiwan

[2]Department of Applied Mathematics, Feng Chia University, Taichung 40724, Taiwan

[3]Center for Micro/Nano Science and Technology, National Cheng Kung University, Tainan 70101, Taiwan

*To whom correspondenec should be addressed. E-mail: hteng@mail.ncku.edu.tw, Tel: 886-6-2385371, Fax:886-6-23444

Electronic Supplementary Information available:

1. The pore size distributions of the carbons on the basis of incremental pore volume;
2. the incremental capacitance values contributed by pores of varying sizes;
3. the ion radii of electrolyte ions.

1. The pore size distributions of the carbons on the basis of incremental pore volume

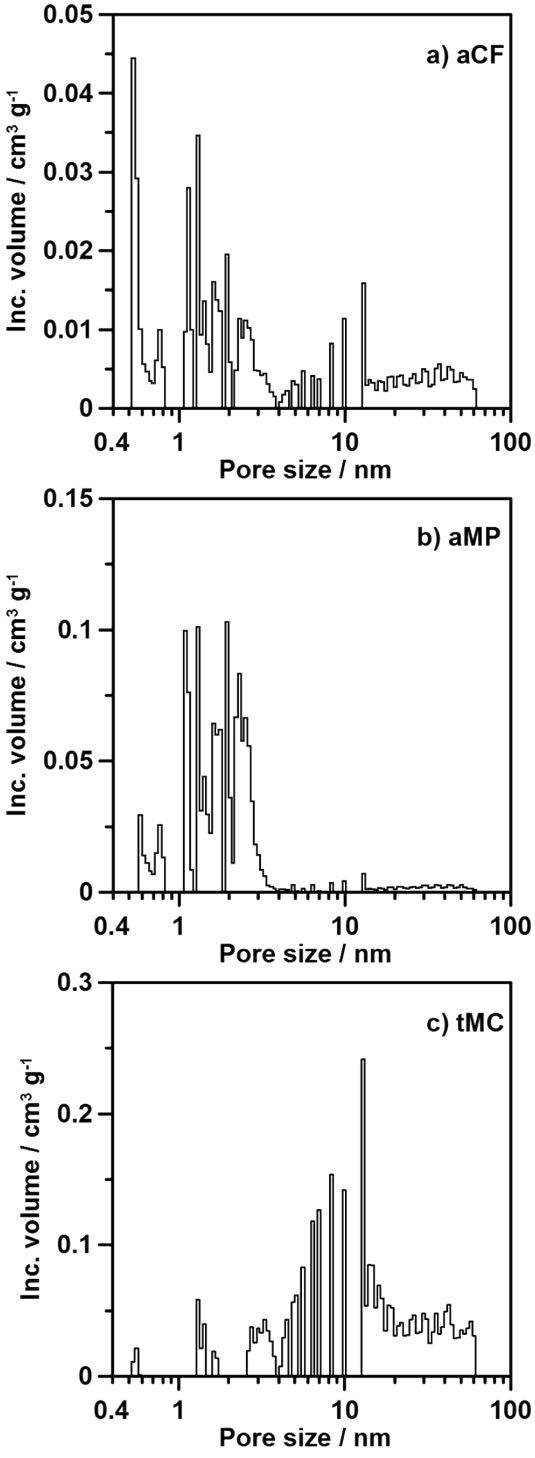

Fig. S1 The pore size distributions of the carbons presented in terms of incremental pore volume: (a) aCF; (b) aMP; (c) tMC.

2. The incremental capacitance values contributed by pores of varying sizes

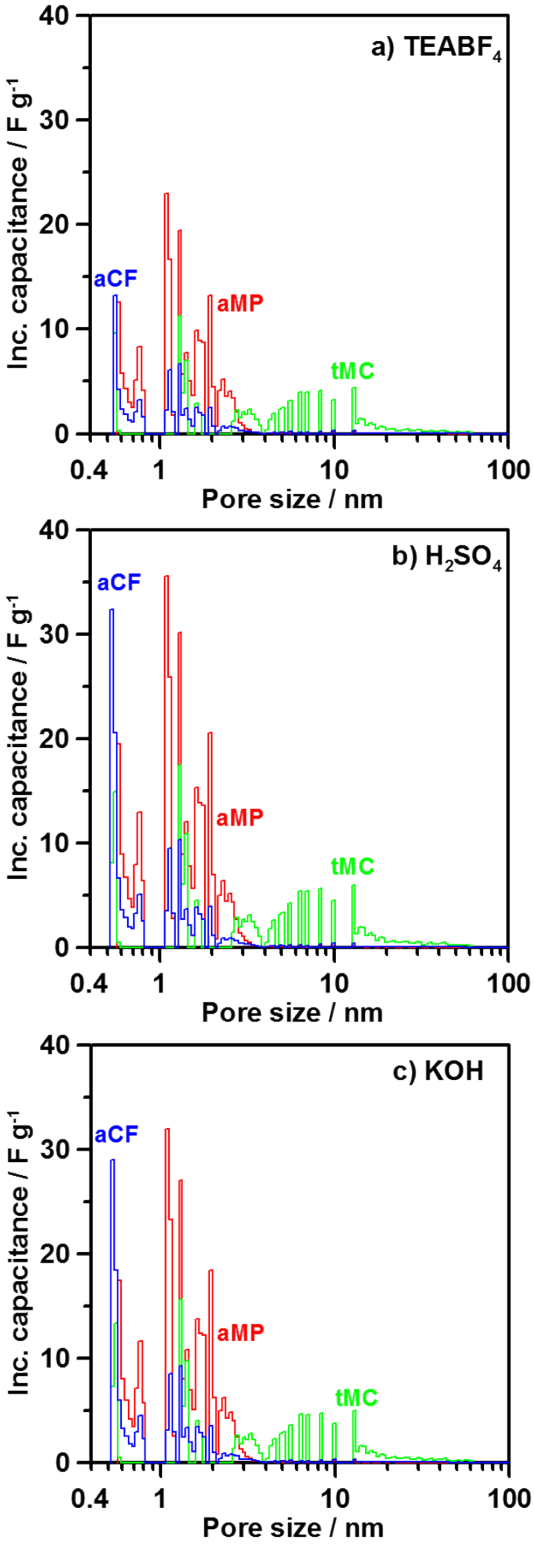

Fig. S2 The incremental capacitance values contributed by pores of varying sizes for different carbons: (a) aCF; (b) aMP; (c) tMC.

3. The ion radii of electrolyte ions

Table S1 The ion radii and mean ion radii of the electrolyte ions used in the present study

	Ion radius (nm)		Mean ion radius, a_0 (nm)
	cation	anion	
$TEABF_4$[1-4]	0.337	0.218,	0.278
H_2SO_4[1,2]	0.028	0.240	0.134
KOH[1,2]	0.138	0.133	0.136

References

1. J. Huang, B. G. Sumpter and V. Meunier, *Chem.–Eur. J.*, 2008, **14**, 6614-6626
2. Y. Marcus, *Biophys. Chem.*, 1994, **51**, 111-127
3. D. Jiang, Z. Jin, D. Henderson and J. Wu, *J. Phys. Chem. Lett.*, 2012, **3**, 1727–1731
4. G. Feng, J. Huang, B. G. Sumpter, V. Meunier and R. Qiao, *Phys. Chem. Chem. Phys.*, 2010, **12**, 5468-5479